Title

Amorphous carbon-coated TiO2 nanocrystals for improved lithium-ion battery and photocatalytic performance

Authors

Xia, Ting
Zhang, Wei
Wang, Zhihui
et al.

Publication Date

2014-05-01

DOI

10.1016/j.nanoen.2014.03.012

Peer reviewed

Amorphous Carbon-Coated TiO_2 Nanocrystals for Improved Lithium-Ion Battery and Photocatalytic Performance

Ting Xia,[1,‡] Wei Zhang,[2,‡] Zhihui Wang,[2] Yuliang Zhang,[1,3] Xiangyun Song,[2] James Murowchick,[4] Vincent Battaglia,[2] Gao Liu,[2,*] Xiaobo Chen[1,*]

[1]Department of Chemistry, University of Missouri – Kansas City, Kansas City, Missouri 64110, USA. [2]Lawrence Berkeley National Laboratory, Berkeley, California, 94720, USA. [3]Institute of Materials Science and Engineering, Shanghai Maritime University, Shanghai, 201306, P. R. China. [4]Department of Geosciences, University of Missouri – Kansas City, Kansas City, Missouri 64110, USA.

KEYWORDS TiO_2 nanocrystals, amorphous carbon coating, lithium ion battery, photocatalytic performance.

ABSTRACT: 10-time lithium rate improvement and 4-time photocatalytic performance enhancement have been achieved with TiO_2 nanocrystals when coated with a thin layer of amorphous carbon from a vacuum decomposition-deposition process. The enhanced performances can be attributed to lower lithium ion diffusion and electronic conduction resistance across the carbon layer into the TiO_2 electrode material and better surface adsorption of the dye molecules and ions. Thus, the current study may provide us an alternative approach in improving the performances of TiO_2 nanocrystals in both lithium ion battery and photocatalysis applications.

INTRODUCTION

Attracted tremendous research effort as a photocatalyst for photocatalytic water splitting and environmental pollutant removal,[1-7] TiO_2 has also been studied as a promising anode material for lithium ion batteries,[7-15] based on the following reaction:

$$xLi^+ + TiO_2 + xe^- \leftrightarrow Li_xTiO_2 \quad (1)$$

where x is the mole fraction of lithium in the titanium dioxide. It has a theoretical capacity up to 335 $mAhg^{-1}$, or 1.0 Li per TiO_2.[7-15] However, for bulk anatase TiO_2, x = 0.5 is usually reported as the maximum,[15,16] due to that the low diffusion coefficient and the low electronic conductivity in the solid phase limits only a thin surface layer of the host material available for Li intercalation at high charging–discharging rates for bulk materials.[11-13] On the other hand, successful realization electric vehicle with long-range single-charge capability requires high-power high-energy batteries with fast charge/discharge rates and high capacity.[17-19] Decreasing the particle size into the nanometer-regime can shorten the lithium diffusion length requirements, alter the electrochemical reactions and reactivity to Li, and thus increase the accessible volume to near-full capacity.[20-23] The size reduction along with unique morphologies may lead to increased capacity beyond 0.5 Li per unit formula based on the different Li-reaction and surface-confined charge storage mechanisms from those in the bulk materials.[20] Conductive carbons,[8] carbon nanotubes,[11-13] graphene,[14] and RuO_2 (with much more improved conductivities),[20] have been used to improve the electronic conduction paths in the host material. However, poor rate performance still seems to be a bottleneck for batteries.

The effective diffusion length of the lithium ions and electrons can be estimated with the formula $L = (Dt)^{1/2}$, where D is the diffusion coefficient, and t is the time.[8] Usually, the Li^+ ion diffusion coefficient is much smaller than that of electrons. For example, the measured diffusion coefficient for Li^+ ion and electrons is 10^{-11} – 10^{-13} cm^2s^{-1} and D = 3–8 × 10^{-6} cm^2s^{-1}, respectively, for TiO_2 material.[11-13] Thus, the main limiting factor in the charge diffusion in the electrode material is mainly from the sluggish transport of the lithium ion. The effective diffusion length for lithium ions is 24 – 240 nm under the charge/discharge rate of 1C and 3.2 – 32 nm under 60C. From this estimation, we can see that full capacity should be achieved if the particle diameter of the electrode is smaller than the above values. This belief has driven intense research in nanomaterials electrode materials research.[8,9] However, many nanomaterials-based electrodes still display performance poorer than expected. This observation hints that other factors such as the lithium ion transfer across the interface may contribute to the limited battery performance. If this speculation is correct, we can expect better battery performance by lowering the interfacial transfer resistance.

Here we demonstrate that lower Li^+ interfacial transfer resistance can be achieved by better adsorption on the electrode-electrolyte interface by coating the electrode with a thin layer of amorphous carbon. The lithium ion battery performance of crystalline TiO_2 nanocrystals can thus be dramatically enhanced. The amorphous carbon layer, mostly porous, possesses better adsorption capability of ions and molecules to facilitate Li^+ transfer across

the electrolyte/TiO_2 interface, due to higher local concentration. Meanwhile, the better adsorption of molecules also benefits the photocatalytic performance as adsorption is normally the first step in the photocatalysis and the amorphous carbon layer can act as an efficient electron trapper to induce better charge separation capability of the carbon-TiO_2 composite, thus increasing the photocatalytic performance.

EXPERIMENTAL SECTION

Nanocrystal synthesis. Crystalline and surface-disordered TiO_2 nanoparticles were prepared as follows. Briefly, crystalline TiO_2 nanoparticles were synthesized from a precursor solution consisting of titanium tetraisopropoxide, ethanol, hydrochloric acid, deionized water, and a polymer template, Pluronic F127. The solution was maintained at 40 °C for 24 hours and then dried at 110 °C. The dried powders were and divided into two parts. One part was calcinated in air at 500 °C for 6 hours to remove the polymer template and to enhance the crystallization of TiO_2 nanoparticles. The calcinated TiO_2 nanocrystals and the other uncalcinated part were put into two separate beakers in one oven and heated under vacuum at 600 ºC for 4 hours. The decomposition of the uncalcinated TiO_2 precursor deposited a thin-layer of amorphous carbon on the surface of the crystalline TiO_2 nanocrystals to obtain the carbon-coated (C-coated) TiO_2 nanocrystals.

Nanocrystal characterization. The TEM study was performed on a FEI Tecnai F20 TEM. The electron accelerating voltage was at 200 kV. Small amount of sample was first dispersed in water and then dropped onto TEM grids. The grids were then dried at 60 ºC overnight before TEM examination. The PXRD was performed using a Rigaku Miniflex PXRD machine with Cu Kα as the X-ray sources (wavelength = 1.5418 Å) and the 2-theta range was from 15º to 80º with a step width of 0.08 and count time of 3 sec/step. The Raman spectra were collected on an EZ-Raman-N benchtop Raman spectrometer (Enwave Optronics, Inc.). The Raman spectrometer is equipped with a 300 mW diode laser and the excitation wavelength is 785 nm. The spectrum range was from 100 cm^{-1} to 3100 cm^{-1}. The spectrum collection time was 4 seconds and was averaged over three measurements to improve the signal-to-noise ratio. The TGA experiments were performed on an SDT-Q600 analyzer (TA Instruments Inc.) instrument in flowed air environment, the temperature range was from room temperature to 1000°C at a ramp rate of 5°C/min. The FTIR spectra were obtained on a Nicolet 6700 FT-IR Spectrometer with an attenuated total reflection (ATR) unit.

Electrode preparation. Half cells were fabricated as follows.[24,25] The materials used in the fabrication of these half cells included acetylene black (AB), polyvinylidene fluoride (PVDF) and N-methylpyrrolidone (NMP). The preparation of the TiO_2 electrodes was conducted in an argon-filled glove box. The electrode mixture (82 wt% TiO_2, 8 wt% AB and 10 wt% PVDF) was steadily dispersed in NMP using a Polytron PT10-35 homogenizer at 2700 rpm for 30 minutes. The slurry was cast on a battery-grade copper sheet using a doctor blade. After being dried overnight, the electrodes were punched to 1/2" diam. discs and dried in *vacuo* at 110°C overnight before being assembled into coin cells. The electrode loading was controlled at around 1.15 mg TiO_2/cm^2.

Coin cell fabrication and testing. Coin cell assembly was prepared in standard 2325 hardware under dry argon atmosphere. The separator was from Celgard (product 2400). 1M lithium hexafluorophosphate ($LiPF_6$) in ethylene carbonate (EC): diethyl carbonate (DEC) (1:2 weight ratio) was used as the electrolyte solution, and lithium as the counter electrode. Cells were discharged to 0.95 V and charged to 3.05 V after 15 min resting for the first cycle at C/25 (calculated from a specific capacity value of 336mAh/g) using a Maccor battery cycler at 30°C. For the 2nd cycle, cells were discharged to 1.0 V and charge to 3.0 V at C/5. Then the cells were cycled at 1C from 1.0 V to 3.0 V. One data point was recorded every 10 mV of voltage change. For the first 18 cycles of the rate performance test, the charge and discharge rates were changed simultaneously; and for the following cycles only the charging rates changed while the discharge rate was kept at 1C.

Electrochemical impedance spectroscopy (EIS) measurement. The EIS measurements were perfomed on a Biologic potentiostat/EIS instrument. The frequency range was between 1 MHz and 10 mHz. The voltage modulation applied was 100 mV. All cells were cycled for two cycles at 1C and 50% discharged before EIS measurements.

Photocatalytic decomposition of methylene blue (MB) and rhodamine B (RB). The photocatalytic activities of the samples were determined by measuring the photocatalytic decomposition process of MB and RB under simulated solar light irradiation. The solar simulator (81094, Newport) has a 150 watt Xe lamp with an AM 1.5 air mass filter. 1.0 mg of catalyst was added into 3.0 ml MB or RB solution (optical density of 1.0). The UV-vis absorption spectrum of MB or RB was monitored over time after the photocatalytic reaction started. The UV-vis spectrum was measured with an Agilent Cary 60 UV-Vis spectrometer with a spectrum range of from 400 nm to 800 nm.

RESULTS AND DISCUSSION

Nanocrystal properties. To confirm the formation of an amorphous layer on the surface of the crystalline TiO_2 nanocrystals, we performed transmission electron microscopy (TEM) studies on both samples (Figure 1). The low resolution TEM images showed that the bare TiO_2 nanocrystals had a primary particle size in the range of 8 – 15 nm in diameter (Figure 1A). The selected area electron diffraction pattern (SAED) of the bare TiO_2 nanocrystals showed clear anatase diffraction rings made of clean diffraction dots, suggesting the highly crystalline nature of the nanocrystals (Inset in Figure 1A). The high-resolution TEM (HRTEM) image (Figure 1B) suggested the bare TiO_2 nanocrystals were highly crystalline throughout the whole particle. The low resolution TEM images showed that the C-coated TiO_2 nanocrystals had a similar particle size in the range of 8 – 15 nm in diameter (Figure 1C), and the milky diffraction background besides

the anatase diffraction rings observed in the SAED suggested the existence of the amorphous carbon layer.[26,27] The HRTEM image in Figure 1D apparently suggested that in the C-coated TiO_2 nanocrystals, the TiO_2 nanocrystals were coated with a layer of amorphous carbon or embedded within the amorphous carbon matrix. This displayed the successful coating of the TiO_2 nanocrystals with an amorphous carbon layer.

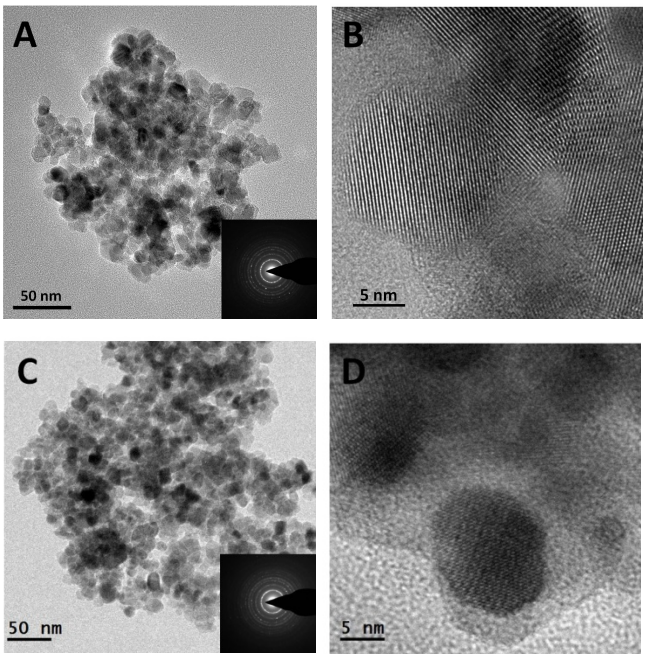

Figure 1. TEM images with SAED patterns, and HRTEM images of bare (A, B) and C-coated (C, D) TiO_2 nanocrystals, respectively.

We also performed the structural characterization of the samples with X-ray diffraction (XRD). The spectra were normalized to the (101) peak with 2θ around 25.3°. The strong diffraction peaks of the XRD suggest that both TiO_2 nanocrystals had highly crystalline anatase phases (Figure 2A). We estimated the particle size with the Scherrer equation: $\tau = (K\lambda)/(\beta\cos\theta)$, where τ is the mean size of the ordered (crystalline) domains, which may be smaller or equal to the grain size, K is the shape factor with a typical value of 0.9, λ is the X-ray wavelength, β is the line broadening full width at half maximum (FWHM) peak height in radians, and θ is the Bragg angle.[28,29] The size of both nanocrystals was similar, around 11 nm when calculated from the (100) peak. We further conducted comparative Raman measurements on both samples. A very weak peak at around 148.7 cm^{-1} (E_g) with a large featureless background was observed for the carbon-coated TiO_2 nanocrystals, compared to the strong characteristic vibrational modes of anatase for the bare TiO_2 nanocrystals at 144.6 cm^{-1} (E_g), 199.1 cm^{-1} (E_g), 397.8 cm^{-1} (B_{1g}), 519.2 cm^{-1} (A_{1g} + B_{1g}), and 641.6 cm^{-1} (E_g) (Figure 2B).[5,30-32] The large background in the Raman spectroscopy suggested a thin layer of amorphous carbon possibly existed on the surface of the C-coated TiO_2 nanocrystals, as Raman is more sensitive to the surface, and XRD tells more about the bulk.[5,30-32]

To find out how much carbon was coated on the TiO_2 nanocrystals, we did thermal gravimetric analysis (TGA) measurements on both samples. The TGA were conducted under air atmosphere from room temperature to 1000 °C (Figure 2C). The 1.2 wt% weight loss below 220 °C was attributed mainly to the water physically or chemically adsorbed on the surface or trapped inside the porous amorphous carbon layer. The 4.9 wt% weight loss between 220 °C and 412 °C was attributed to the decomposition of the porous amorphous carbon layer (4.6 wt%) and loss of OH groups (0.3 wt%) on the TiO_2 nanocrystals. The slight weight change above 412 °C was mainly due to the phase transition of the TiO_2 nanocrystals. Thus, the total amount of carbon deposited on the TiO_2 nanocrystals was about 4.6 wt%.

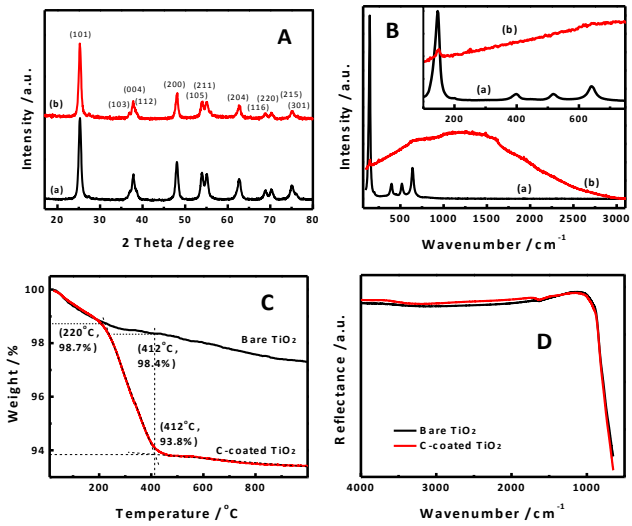

Figure 2. (A) XRD and (B) Raman spectra of bare (curves a) and C-coated TiO_2 nanocrystals (curves b), (C) TGA and (D) FTIR spectra of bare and C-coated TiO_2 nanocrystals.

In order to check if there are any organic residues left in the amorphous carbon layer formed by decomposing the organic template and the TiO_2 precursor at high temperature in vacuum, we measured the Fourier-transform infrared spectrum of the C-coated TiO_2 nanocrystals in comparison with bare TiO_2 nanocrystals. Both samples displayed similar Fourier transform infrared spectroscopy (FTIR) spectra (Figure 2D): a broad adsorption band center at 3400 cm^{-1} from the O–H stretch modes of the surface hydroxyl groups with hydrogen bonds and chemisorbed water and the peak centered at 1630 cm^{-1} from O–H bending of physisorbed water.[33-35] The slightly large OH bands in the C-coated TiO_2 nanocrystals suggest that its OH content was slightly higher than the bare TiO_2 nanocrystals.

Lithium-Ion Battery Performance. In order to test the concept of the stabilization of the lithium insertion and extraction with the C-coated TiO_2 nanocrystals, we fabricated half cells and tested their performances. In the half cell configuration, lithium metal was used as the an-

ode, and TiO_2 nanocrystals were used as the cathode materials. The discharge and charge corresponded to the lithium insertion and extraction, respectively. The theoretical specific capacity value of 336 mAh/g was used for C-rate calculation. The half cells were initially discharged to 1.0 V and charged to 3.0 V after 15 min resting for the first cycle at C/25. For the 2nd cycle, the cells were discharged and charge at C/5. Finally the cells were cycled at 1C. The initial discharge capacity of the C-coated TiO_2 nanocrystals was 278 mAh/g at C/25 rate, 211 mAh/g at C/5 rate, 178 mAh/g at 1C rate for the first, second, and third cycle, respectively, 17%, 30% and 29% higher that of the bare TiO_2 nanocrystals (237 mAh/g, 162 mAh/g and 138 mAh/g) (Figure 3A). After 100 cycles, the discharge capacity of the C-coated TiO_2 nanocrystals was 166 mAh/g at 1C rate, 47% higher than that of the crystalline TiO_2 nanocrystals (113 mAh/g). The C-coated TiO_2 nanocrystals displayed 93% capacity retention rate after 100 cycles at 1C rate, compared to the 82% retention rate of the bare TiO_2 nanocrystals. The discharge capacity of the C-coated TiO_2 nanocrystals after 100 cycles at 1C rate was even higher than that of the initial capacity of the bare TiO_2 nanocrystals at C/5 rate: a 5 times rate performance increase.

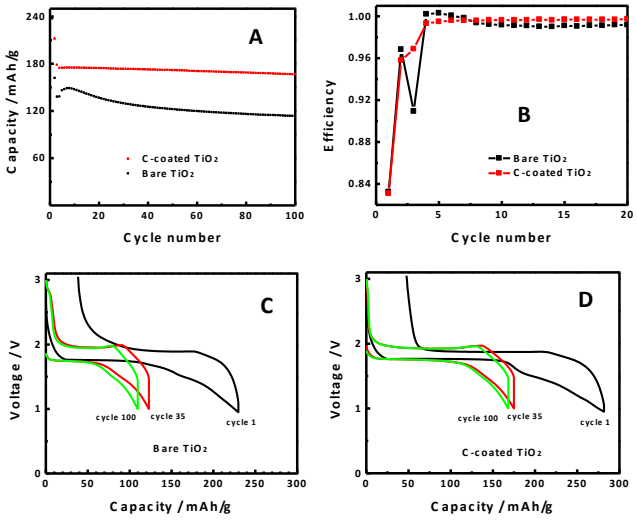

Figure 3. (A) Variation of discharge capacity versus cycle number for the first 100 cycles and (B) Variation of Coulombic efficiency along with the charge/discharge versus cycle number for the first 20 cycles, for bare and C-coated TiO_2 nanocrystals. Galvanostatic charge/discharge profiles at first cycle at C/25 rate, 35th cycle at 1C rate, and 100th cycle at 1C rate for the electrode made of bare (C) and C-coated TiO_2 nanocrystals (D).

Better Coulombic efficiency was observed for the C-coated TiO_2 nanocrystals over the bare TiO_2 nanocrystals. The Coulombic efficiency here was defined as the ratio of charge (lithium extraction) capacity/discharge (lithium insertion) capacity. A closer look at the first 20 cycles revealed that the discharge efficiency increased with large fluctuation for the bare TiO_2 nanocrystals in the first four cycles followed by slight decrease in the next 16 cycles, while the discharge efficiency of and the C-coated TiO_2 nanocrystals increased steadily to the maximum within the first 5 cycles and followed with steady maximum efficiency in the next 15 cycles (Figure 3B). The bare TiO_2 nanocrystals showed a quick drop of the discharge efficiency in the initial stage followed by a climb-up to the efficiency of around 99.5% after the first 30 cycles which is steady afterward for the remaining 70 cycles; the C-coated TiO_2 nanocrystals show a rapid climb in the initial 5 cycles to the efficiency of around 99.7% which is steady afterward for the remaining 95 cycles (Figure S1). The large fluctuation in the discharge efficiency of the bared TiO_2 nanocrystals could be due to structural struggling to form a stable solid-electrolyte interface (SEI) layer at the initial cycles in the charge/discharge process, while the quick and steady ramp up of the discharge efficiency of the C-coated TiO_2 nanocrystals suggested a better formation of SEI layer and a smaller charge transfer resistance across the interface.

Besides the larger charge/discharge capacity at various cycles, the C-coated TiO_2 nanocrystals showed longer charge/discharge plateaus and smaller potential difference between the charge and discharge cycle. The potential difference between the first charge and discharge cycle of the C-coated TiO_2 nanocrystals was about 0.10 V, 47% smaller than that of the bare TiO_2 nanocrystals of about 0.19 V (Figures 3C and 3D). This smaller potential difference indicated decreased charge transport resistance across the interface and even in the TiO_2 nanocrystalline lattice. The longer charge/discharge plateaus suggested that more host matrix materials were efficiently involved with the charge insertion/distraction in the charge/discharge processes. Overall, the charge transfer was smoother for the C-coated TiO_2 nanocrystals than for the bare TiO_2 nanocrystals.

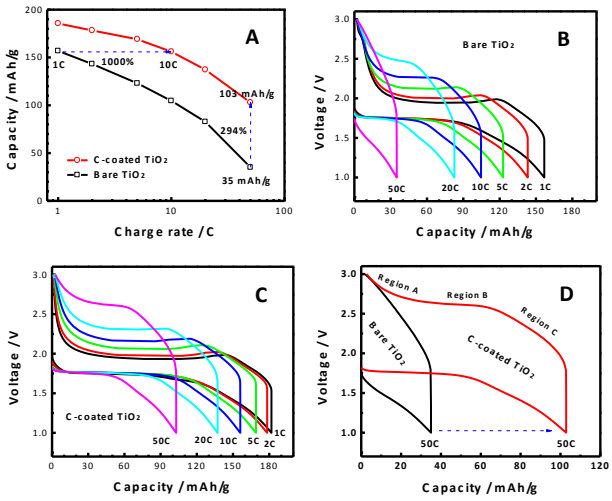

Figure 4. (A) Rate performances of the bare and C-coated TiO_2 nanocrystals. Galvanostatic charge/discharge profiles at various charge (lithium extraction) rates for the electrode made of the bare (B) and C-coated TiO_2 nanocrystals (C). (D) Comparison of the charge/discharge profiles for bare and C-coated TiO_2 nanocrystals at charge rates of 50C.

We tested the rate performance of the bare TiO_2 nanocrystals and the C-coated TiO_2 nanocrystals under varied charge rates (Figure 4A). The discharge (lithium insertion) rate was kept at 1C and only the charge (lithium extraction) rate changed. The C-coated TiO_2 nanocrystals showed much better performance over the crystalline TiO_2 under the same testing condition. The capacity of C-coated TiO_2 was 186 mAh/g at 1C, 156 mAh/g at 10C, and 103 mAh/g at 50C, 118%, 149% and 294% as that of bare TiO_2 at the same conditions (157 mAh/g at 1C, 105 mAh/g at 10C, and 35.0 mAh/g at 50C), respectively. At higher charge rates, the improvement was more apparent for the C-coated TiO_2 over the crystalline TiO_2. The C-coated TiO_2 nanocrystals sustained much higher charge rate than crystalline TiO_2 nanocrystals. It would take around 1 hour (1C) to charge with bare TiO_2 nanocrystals to 150 mAh/g capacity, but only 6 min (~10C) for C-coated TiO_2 nanocrystals. Thus, the charge rate of the C-coated TiO_2 is 10 times as that of bare TiO_2. Testing under simultaneously changed discharge/charge rate displayed similar rate performance (Figure S2). The higher rate performance of the C-coated TiO_2 nanocrystals was possibly due to the lower energy barrier of the lithium ion transport across interface.

The galvanostatic charge/discharge profiles at various charging rates for the electrode made of bare and C-coated TiO_2 nanocrystals were shown in Figures 4B and 4C, respectively. The C-coated TiO_2 nanocrystals showed higher capacity and larger charge/discharge plateaus over the bare TiO_2 at each charging rate. The larger charge/discharge plateaus indicated that smoother charge transport between the host matrix and the transferred charges. The discharge curve for the nanoporous anatase electrode can be divided into three different voltage regions (Figure 4D).[20,36-38] A monotonic voltage drop to ≈ 1.75 V occurs in region A, which is attributed to a homogeneous Li insertion into the bulk, up to a solid-solution limit of Li in TiO_2.[20,36-38] A typical biphase plateau (region B) is observed at a potential of ≈ 1.75 V, where Li-rich phases are expected to coexist with the Li-poor TiO_2 phase. Further reversible storage of Li is able to occur at particle interfaces in this voltage region, representing region C.[20] At voltages over 1.75 V, the phases no longer reversibly dissolve Li, although more Li can be accommodated by further two-phase bulk intercalation ($x > 0.5$). As reported previously, Reducing the particle size is indeed effective in improving both the bulk intercalation and the interfacial storage capacities, leading to an increase of region B (due to the shorter diffusion length) and C (due to the larger interfacial area), with a slight increase in the proportion of region C.[20] Thus, the high surface area of the nanometer-sized TiO_2 provided many available extra sites for lithium accommodation at interfaces (interfacial storage), beyond the fraction of octahedral sites available for the lithium-intercalation reaction in the bulk.[20]

In order to analyze why the charge transfer/transport across the crystalline matrix was facilitated through a thin layer of amorphous carbon coating, electrochemical impedance spectra (EIS) were measured on both samples under the same condition (Figure 5A). Both cells were cycled for two cycles and 50% discharged before EIS measurements. The equivalent circuit modeling[39] and fitting results (Figure 5B) suggested that the charge transfer and transport resistance was largely reduced for C-coated TiO_2 nanocrystals compared to bare TiO_2 nanocrystals. First, the ohmic resistance was slightly reduced for the C-coated TiO_2 nanocrystals, suggesting better electrical contacts between the electrode materials and the copper foil. The double layer charge capacitances in both carbon/electrode (C_1) and TiO_2 electrode/carbon (CPE–T) interfaces were similar. The electron transfer resistance across the interfaces (R_1) was reduced in the C-coated TiO_2 to 4.1 Ω from 5.6 Ω of bare TiO_2. The Li^+ transfer resistance across TiO_2 electrode/electrolyte interface (R_{CPE}) was largely reduced from 104.7 of bared TiO_2 to 48.2 Ω of C-coated TiO_2. The lowered Li^+ transfer resistance could be due to the slightly higher Li^+ concentration near the TiO_2 electrode as seen from the slightly higher double layer capacitance (CPE-T). The charge transport/diffusion resistance (W_o-R) in the C-coated TiO_2 electrode was smaller (41.6 Ω) than that in bare TiO_2 electrode (56.5 Ω). The smaller charge diffusion resistance could be attributed to the possibly oxygen vacancy created during the vacuum carbon deposition process by the reduction of TiO_2 with carbon at high temperature,[40] as oxygen vacancy has been shown to lower the charge transfer resistance due to improved electrical conductivity.[20,41]

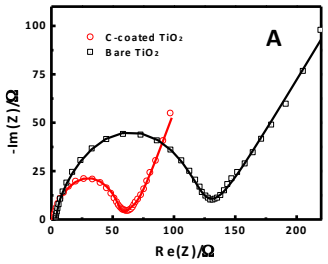

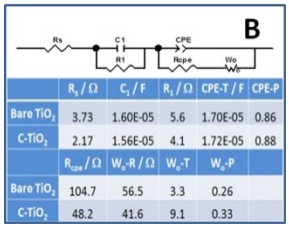

	R_s / Ω	C_1 / F	R_1 / Ω	CPE-T / F	CPE-P
Bare TiO_2	3.73	1.60E-05	5.6	1.70E-05	0.86
C-TiO_2	2.17	1.56E-05	4.1	1.72E-05	0.88
	R_{cpe} / Ω	W_o-R / Ω	W_o-T	W_o-P	
Bare TiO_2	104.7	56.5	3.3	0.26	
C-TiO_2	48.2	41.6	9.1	0.33	

Figure 5. (A) EIS spectra of bare and C-coated TiO_2 nanocrystals. (○) and (□) are the raw data, the lines are the fitted curves. (B) The equivalent circuit used to fit the EIS spectra and the fitted values for the corresponding components in the circuit. **Rs**: ohmic resistance, including the bulk resistance of the electrolyte, separator, and electrode; **R_1**: electron transfer resistance at the TiO_2/carbon/electrolyte interface; **C_1**: double layer charge capacitance in the carbon/electrode interface. **CPE–T:** time constant component of the constant phase element (CPE), approximate to the double layer charge capacitance in the TiO_2/electrolyte interface; **CPE–P:** the exponential part of the constant phase element; **R_{CPE}**: Li^+ transfer resistance cross the TiO_2/electrolyte interface; **W_o-R**: Warburg charge diffusion resistance in the TiO_2 electrode; **W_o-T**: Warburg diffusion time = L^2/D in the electrode, L is the length of the diffusion layer in the electrode, and D is the diffusion coefficient in the electrode; **W_o-P**: Warburg exponent.

Photocatalytic performance. To reveal their photocatalytic and surface adsorption activity, we conducted pho-

tocatalytic decomposition of methylene blue (MB) and rhodamine B (RB) solution with both samples under simulated solar light irradiation. The UV-vis absorption spectra of MB and RB were monitored over time after the photocatalytic reaction started. The MB solution quickly lost its color in the short course of 10 minutes irradiation with the C-coated TiO_2 nanocrystals as catalyst (Figures 6A and S3), indicating most of the MB was decomposed. It took about 40 minutes for the pristine TiO_2 nanocrystals to decompose the same amount of MB molecules under the same condition. This suggested that C-coated TiO_2 nanocrystals had an about four-fold better photocatalytic activity than pristine TiO_2 nanocrystals in decomposing MB. It took around 40 minutes for the C-coated TiO_2 nanocrystals to decolor the RB solution, while a large amount of RB still remained after 60 minutes' irradiation with pristine TiO_2 nanocrystals (Figures 6B and S4). Apparently, C-coated TiO_2 nanocrystals displayed much higher activity in decomposing RB as well.

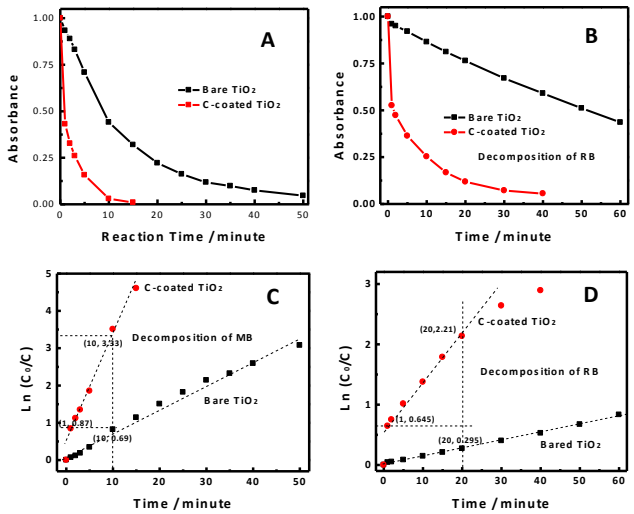

Figure 6. (A) The maximum optical absorbance change of methylene blue and (B) rhodamine B solution as a function of solar irradiation time with pristine and C-coated TiO_2 nanocrystals. (C) $Ln(C_o/C)$ of methylene blue and (D) rhodamine B as a function of solar irradiation time with pristine and C-coated TiO_2 nanocrystals.

When the initial concentration of dye is very small, the degradation of dyes can be described by an apparent first-order equation with a simplified Langmuir-Hinshelwood model:

$$\ln(C_o/C) = k_a t \qquad (2)$$

where C_o is the initial concentration of dye, k_a is the apparent first-order rate constant, C is the concentration of the dye and t is the illumination time.[42,43] The slope of the $\ln(C_o/C)$ ~ t tells the rate constant of the reaction, and the incept on the y axis tells the amount of adsorption. The $Ln(C_o/C)$ ~ t plots in Figures 6C and 6D showed that the rate constant of the C-coated TiO_2 nanocrystals (16.4/h) was almost 4 times of the bare TiO_2 nanocrystals (4.14/h) in decomposing MB, and 5.5 times (4.9/h vs. 0.89/h) in decomposing RB. The incept on the y axis suggested that the surface adsorption was much obvious for C-coated TiO_2 nanocrystals than for the bare TiO_2 nanocrystals. The improvement of the photocatalytic activity of the C-coated TiO_2 nanocrystals was likely due to the better dye adsorption on the surface and faster decomposition possibly from the better charge separation efficiency from the C-TiO_2 interfacial heterojunction. The better dye adsorption capability of the C-coated TiO_2 also suggested its better Li^+ adsorption as the color centers of the both dyes are cationic. This could increase the local Li^+ near and the Li^+ transfer across the TiO_2/electrolyte interface.

CONCLUSIONS

We have demonstrated successfully that a thin layer of amorphous carbon can be created on crystalline TiO_2 nanocrystals with a vacuum decomposition-deposition process. We evaluated the C-coated TiO_2 nanocrystal as an electrode material for lithium ion batteries and found it exhibited greatly improved lithium insertion/extraction performance compared with crystalline TiO_2, and showed an excellent rate capability improvement (103 mAh/g vs. 35 mAh/g at 50C, and 10C vs. 1C at around 156 mAh/g). We also studied their photocatalytic performance and found the C-coated TiO_2 nanocrystal displayed over 4 times improvements in decomposing organic dye molecules (MB and RB), besides the better adsorption capability, over bare TiO_2 nanocrystal. We attributed the greatly enhanced lithium storage properties of the C-coated TiO_2 nanocrystals to the lower lithium ion diffusion and electronic conduction resistance and better surface adsorption in the amorphous carbon layer. Thus adding a thin layer of amorphous carbon on crystalline materials may be applied as an alternative approach for improving the battery and photocatalytic performance of other materials as well.

ASSOCIATED CONTENT

Supporting Information. Variation of Coulombic efficiency along with the charge/discharge versus cycle number for bare and C-coated TiO_2 nanocrystals; Rate performances of the bare and C-coated TiO_2 nanocrystals. The charge and discharge rate were the same for each cycle; Optical absorbance spectrum change of methylene blue and rhodamine B solution under solar irradiation time using bared and C-coated TiO_2 nanocrystals.

AUTHOR INFORMATION

Corresponding Author

* (G.L.) GLiu@lbl.gov.
* (X.C.) chenxiaobo@umkc.edu

Author Contributions

‡ T. Xia and W. Zhang contributed equally to this work.

ACKNOWLEDGMENT

G. L. thanks the fund by the Assistant Secretary for Energy Efficiency, Office of Vehicle Technologies of the United State Department of Energy under Contract No. DE-AC03-76SF00098. X. C. thanks the support from College of Arts and Sciences, University of Missouri - Kansas City, the University of Missouri Research Board, and the generous gift

from Dow Kokam. Y. Z. thanks National Natural Science Foundation of China (No. 21071096) for its financial support.

REFERENCES

(Word Style "TF_References_Section").

(1) Fujishima, A.; Honda, K. *Nature* **1972**, *238*, 37 – 38.

(2) Choi, W.; Termin, A.; Hoffmann, M. R. *J. Phys. Chem.* **1994**, *98*, 13669 – 13679.

(3) Asahi, R.; Morikawa, T.; Ohwaki, T.; Aoki, K.; Taga, Y. *Science* **2001**, *293*, 269 – 271.

(4) Chen, X.; Mao, S. S. *Chem. Rev.* **2007**, *107*, 2891 – 2959.

(5) Chen, X.; Liu, L.; Yu, P. Y.; Mao, S. S. *Science* **2011**, *331*, 746 – 750.

(6) Chen, X.; Burda, C. *J. Am. Chem. Soc.* **2008**, *130*, 5018 – 5019.

(7) Chen, X.; Li, C.; Gratzel, M.; Kostecki, R.; Mao, S. S. *Chem. Soc. Rev.* **2012**, *41*, 7909 – 7937.

(8) Bruce, P. G.; Scrosati, B.; Tarascon, J.-M. *Angew. Chem. Int. Ed.* **2008**, *47*, 2930 – 2946.

(9) Xia, T.; Zhang, W.; Li, W.; Oyler, N. A.; Liu, G.; Chen, X. *Nano Energy*, **2013**, 2, 826 – 835.

(10) Wagemaker, M.; Kentgens, A. P. M.; Mulder, F. M. *Nature* **2002**, *418*, 397 – 399.

(11) Moriguchi, I.; Hidaka, R.; Yamada, H.; Kudo, T.; Murakami, H.; Nakashima, N. *Adv. Mater.* **2006**, *18*, 69 – 73.

(12) Solbrand, A.; Henningsson, A.; Sodergren, S.; Lindstrom, H.; Hagfeldt, A.; Lindquist, S.-E. *J. Phys. Chem. B* **1999**, *103*, 1078 – 1083.

(13) Abayev1, I.; Zaban, A.; Fabregat-Santiago, F.; Bisquert, J. *Phys. Stat. Sol. (a)* **2003**, *196*, R4 – R6.

(14) Li, N.; Liu, G.; Zhen, C.; Li, F.; Zhang, L.; Cheng, H.-M. *Adv. Funct. Mater.* **2011**, *21*, 1717 – 1722.

(15) Lindström, H.; Södergren, S.; Solbrand, A.; Rensmo, H.; Hjelm, J.; Hagfeldt, A.; Lindquist, S.-E. *J. Phys. Chem. B* **1997**, *101*, 7717 – 7722.

(16) van de Krol, R.; Goossens, A.; Meulenkamp, E. A. *J. Electrochem. Soc.* **1999**, *146*, 3150 – 3154.

(17) Armand, M.; Tarascon, J. M. *Nature* **2008** , *451*, 652 – 657.

(18) Tollefson, J.; Scully, T.; Witze, A.; Morton, O. *Nature* **2008**, *454*, 818 – 822.

(19) Cao, Y. L.; Xiao, L. F.; Wang, W.; Choi, D.; Nie, Z. M.; Yu, J. G.; Saraf, L. V.; Yang, Z. G.; Liu, J. *Adv. Mater.* **2011**, *23*, 3155 – 3160.

(20) Shin, J.-Y.; Samuelis, D.; Maier, J. *Adv. Funct. Mater.* **2011**, *21*, 3464 – 3472.

(21) Wagemaker, M., Borghols, W. J. H., Mulder, F. M. *J. Am. Chem. Soc.* **2007**, *129*, 4323 – 4327.

(22) Kavan, L.; Kalbac, M.; Zukalova, M.; Exnar, I.; Lorenzen, V.; Nesper, R.; Gräetzel, M. *Chem. Mater.* **2004**, *16*, 477 – 485.

(23) Kim, J.; Cho, J. *J. Electrochem. Soc.* **2007**, *154*, A542 – A546.

(24) Xun, S.; Song, X.; Grass, M. E.; Roseguo, D. K.; Liu, Z.; Battaglia, V. S.; Liu, G. *Electrochem. Solid-State Lett.* **2011**, *14*, A61 – A63.

(25) Liu, G.; Xun, S.; Vukmirovic, N.; Song, X.; Olalde-Velasco, P.; Zheng, H.; Battaglia, V. S.; Wang, L.; Yang, W. *Adv. Mater.* **2011**, *23*, 4679 – 4683.

(26) Fultz, B.; Howe, J. *Transmission Electron Microscopy and Diffractometry of Materials*, Springer, New York, **2009**.

(27) Champness, P. E. *Electron Diffraction in the Transmission Electron Microscope*, Taylor & Francis, **2001**.

(28) Jenkins, R.; Snyder, R. L. *Introduction to X-ray Powder Diffractometry*, John Wiley & Sons Inc., New York, **1996**.

(29) Xia, T.; Otto, J. W.; Dutta, T.; Murowchick, J.; Caruso, A. N.; Peng, Z.; Chen, X. *J. Mater. Res.* **2013,** *28*, 326 – 332.

(30) Kelly, S.; Pollak, F. H.; Tomkiewicz, M. *J. Phys. Chem. B* **1997**, *101*, 2730 – 2734.

(31) Tian, F.; Zhang, Y.; Zhang, J.; Pan, C. *J. Phys. Chem. C* **2012**, *116*, 7515 – 7519.

(32) Zhang, J.; Li, M.; Feng, Z.; Chen, J.; Li, C. *J. Phys. Chem. B* **2006**, *110*, 927 – 935.

(33) Zou, J.; Gao, J.; Xie, F. *J. Alloys Compd.* **2010**, *497*, 420 – 427.

(34) Li, G.; Li, L.; Boerio-Goates, J.; Woodfield, B. F. *J. Am. Chem. Soc.* **2005**, *127*, 8659 – 8666.

(35) Kuvarega, A. T.; Krause, R. W. M.; Mamba, B. B. *J. Phys. Chem. C* **2011**, *115*, 22110 – 22120.

(36) Guo, Y.-G.; Hu, Y.-S.; Maier, J. *Chem. Commun.* **2006**, 2783 – 2785.

(37) Guo, Y.-G.; Hu, Y.-S.; Sigle, W.; Maier, J. *Adv. Mater.* **2007**, *19*, 2087 – 2091.

(38) Hu, Y.-S.; Kienle, L.; Guo, Y.-G.; Maier, J. *Adv. Mater.* **2006**, *18*, 1421 – 1426.

(39) Orazem, M. E.; Tribollet, B. *Electrochemical impedance spectroscopy*, John Wiley & Sons, NJ, USA, **2011**.

(40) Li, Y.; Li, X.; Li, J.; Yin, J. *Mater. Lett.* **2005**, *59*, 2659 – 2663.

(41) Xia, T.; Zhang, W.; Murowchick, J.; Liu, G.; Chen, X. *Adv. Energy Mater.* **2013**, DOI: 10.1002/aenm.201300294.

(42) Mizukoshi, Y.; Ohtsu, N.; Semboshi, S.; Masahashi, N. *Appl. Catal. B* **2009**, *91*, 152 – 156.

(43) Chen, X.; Halasz, S.; Giles, E. C.; Mankus, J. V.; Johnson, J. C.; Burda, C. ***J. Chem. Educ.*** **2006**, *83*, 265 – 267.

SYNOPSIS TOC. 10-time lithium rate improvement and 4-time photocatalytic performance enhancements have been achieved on carbon-coated TiO_2 nanocrystals due to lower interfacial lithium ion diffusion and electronic conduction resistance and better surface adsorption of ions and dye molecules.